IEEE Access
Multidisciplinary ⋮ Rapid Review ⋮ Open Access Journal

Received June 2, 2020, accepted June 9, 2020, date of publication June 15, 2020, date of current version June 24, 2020.

Digital Object Identifier 10.1109/ACCESS.2020.3002172

Research on Fault Location of Process-Level Communication Networks in Smart Substation Based on Deep Neural Networks

BO REN[1,3], JINSONG LI[2,3], YONGKANG ZHENG[1], XIAODONG CHEN[4], YIBING ZHAO[4], HAIYANG ZHANG[1], AND CHAO ZHENG[1]

[1]Sichuan Electric Power Research Institute, State Grid Sichuan Electric Power Company, Chengdu 610041, China
[2]China Electric Power Research Institute, Beijing 100192, China
[3]School of Electrical and Electronic Engineering, North China Electric Power University, Baoding 071003, China
[4]State Grid Sichuan Electric Power Company, Chengdu 610041, China

Corresponding author: Jinsong Li (lijinsong@epri.sgcc.com.cn)

This work was supported in part by the Open Fund of Beijing Key Laboratory of Research and System Evaluation of Power Dispatching Automation Technology under Grant DZB51201901097, and in part by the State Grid Sichuan Electric Power Company 2019 Project under Grant 521997190004.

ABSTRACT With the continuous improvement of substation automation, the number of communication equipment has risen sharply, the network topology is more complicated, and the problem of unable to locate the fault of process-level communication networks quickly and accurately has become more and more prominent. Under this background, to improve the maintenance efficiency of process-level communication networks in the smart substation, this article proposes a method for fault location of process-level communication networks based on deep neural networks. Based on the redundant monitoring of the fault state, the fault feature information of different monitoring nodes in the message transmission process is analyzed, and the characterization method of the fault feature information is proposed accordingly. Based on the emergence principle, it realizes the automatic generation of fault samples according to the physical connection, logical connection, and message subscription relationship of process-level communication networks. Combined with the training rules in deep learning theory, a fault location model of process-level communication networks based on deep neural networks is established, and the real-time location steps are given. Taking the process-level communication network of a typical 110kV smart substation as an example, simulations verify the effectiveness and accuracy of the proposed fault location method in single fault environments and multiple fault environments. Besides, accurate results can be obtained even when the fault feature information is wrong or missing, and the anti-interference ability is excellent.

INDEX TERMS Smart substation, communication networks, fault location, deep neural networks, deep learning.

I. INTRODUCTION

Smart substations have the remarkable characteristics of intelligent main equipment and networked auxiliary equipment [1], [2]. The process-level communication network consisting of fiber-optic links and auxiliary equipment carries the transmission of critical messages such as Sampled Values (SV) and Generic Object Oriented Substation Events (GOOSE). The safety and reliability of the process-level communication network are a powerful guarantee for the stable operation of smart substations [3].

The faults in the process-level communication network mainly occur in the auxiliary equipment ports, switches, and fiber-optic links [4]. Aiming at these faults, the technicians at this stage mostly judge the cause based on the functions such as message records and traffic monitoring in the Network Analyzer (NA). However, due to a large number of equipment ports and the complicated fiber-optic links in the process-level communication network, the types of messages generated become more and more numerous, leading to the loss of many essential messages. Besides,

The associate editor coordinating the review of this manuscript and approving it for publication was Tariq Umer.

the communication between auxiliary equipment depends on the message subscription relationship in the Substation Configuration Description (SCD) file. Still, the SCD file only has the source and destination of the message and does not describe the actual physical connection. Therefore, when a fault occurs on the process-level communication network, the subscriber of the message can only issue an alarm, but cannot locate the fault directly [5]. On this basis, xi proposed parsing GOOSE and SV messages and combined with traffic control, by setting three security lines to ensure the reliable transmission of critical messages [6]. This method can only prevent the communication network from collapsing in a large area, but unable to locate the fault. Li proposed a Shared Risk Link Group (SRLG) weighted p-cycle algorithm (SWCA) to reduce the possibility of simultaneous faults of the working path and the protection path [7]. This method can mitigate the impact of faults to a limited extent. However, the optimization of bandwidth allocation alone cannot fundamentally solve the faults. Luo proposed a flow-criterion method based on communication equipment. Through the switch learning network topology, establishing the relationship between logical connection and physical connection, and counting information of historical traffic to realize fault location [8]. However, the topology structure of the auxiliary system in an actual smart substation has various composition schemes. If part of the message transmission uses a non-networking method, this method fails. Zhang proposed a method based on the cross-path method by using the proof table [9]. However, due to the fault feature information used is too single, this method can only reduce the range of suspicious faults and has the limited anti-interference ability.

In summary, the current methods are unable to locate faults in process-level communication networks quickly and accurately. The reasons are as follows:

1) There are many types of faults in process-level communication networks, but there are fewer criteria, and the correlation between fault features is weak.
2) The connection relationship between equipment is complicated, so traditional methods cannot efficiently and quickly analyze massive multidimensional data.
3) The problems such as distortion and loss that may occur in the process of message transmission cause the results obtained by the above methods to fluctuate with different confidence levels of messages.

Given the shortcomings of the above methods and the reasons analyzed, this article proposes a method for fault location of process-level communication networks in smart substations based on deep neural networks (DNN), which opens a new way to break the bottleneck of current fault location. Based on the redundant monitoring of the fault state of the process-level communication network, the feature information of different monitoring nodes is analyzed, and the characterization method of fault feature information is proposed. Based on the emergence principle, the automatic generation of fault samples is realized based on the physical connection, logical connection, and message subscription relationship of the communication network. Combined with the training rules of deep learning, a DNN-based model of fault location is established. In real-time fault localization, the fault point can be obtained by taking the fault feature information as input and calculating with the DNN location model.

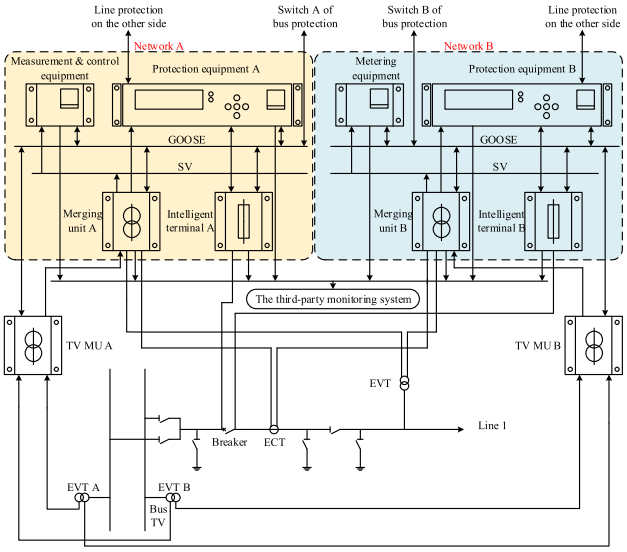

FIGURE 1. Auxiliary system of line 1.

II. ANALYSIS OF FAULT FEATURE INFORMATION

The currently constructed smart substations all comply with the IEC 61850. The smart substations have the process bus and networked auxiliary equipment. However, in practical engineering applications, there are still some differences in the process-level communication networks of smart substations in different countries. The following discussion is based on smart substations in China, as shown in Figure 1, taking the secondary system of Line 1 as an example, the process-level communication network is divided into network A and network B, there is no significant redundancy in a single network, but two completely independent networks and relative auxiliary equipment are configured to ensure the reliability of the secondary system.

So, the main characteristics of the process-level communication network of smart substations in China are:

1) In the network structure, it is specified that the process bus uses the star topology, and other structures such as ring topology are not used.
2) The smart substations adopt two independent sets of protection equipment in any interval, corresponding to two sets of networks.
3) Protection equipment, measurement & control equipment, etc. are independent and diversified.

A. REDUNDANT MONITORING OF FAULT STATE OF PROCESS-LEVEL COMMUNICATION NETWORKS

According to the relationships of message transmission between the auxiliary equipment, the communication

network can be divided into four components, namely the source, the intermediate forwarding equipment (switch), the fiber-optic link, and the destination. When some parts fail, the transmission state of message flow will have different changes, such as the message reception state and the equipment operating state. Therefore, monitoring nodes at various locations in the communication network can be used to monitor the message flow in the fault state redundantly, and the feature information obtained from these nodes is the data foundation that supports accurate fault location.

The monitoring alarms involved in the fault location of the process-level communication network based on different monitoring nodes includes:

1) ALARMS OF ABNORMAL STATE BASED ON THE DESTINATION

Unlike the equipment in the primary system, which requires the separate monitoring equipment to achieve fault location, most of the equipment in the auxiliary system has self-test and communication functions [10], [11]. Therefore, we can know the impact of the communication network fault by deploying monitoring nodes on the destination of messages. When a fault occurs on the fiber-optic link or the forwarding equipment, some of the messages cannot be received regularly. At this time, the monitoring node will issue the abnormal message reception alarm (AMRA). When a fault occurs on the port of auxiliary equipment, in addition to failing to receive some of its subscribed messages regularly, the corresponding faulty equipment will self-check abnormally. In this case, the monitoring node will forward the self-test error alarm (STEA) in addition to the AMRA mentioned above.

2) ALARMS OF ABNORMAL STATE BASED ON THE SWITCH

When the message transmission between the auxiliary equipment adopts the networking method, the stable operation of the switch as the intermediate medium determines the reliability of the networking method. Therefore, by configuring the statistics function of message traffic on the switch, we can obtain the traffic information that characterizes the internal operating state of the process-level communication network [12]. When a fault occurs in the process-level communication network, the traffic of some GOOSE/SV messages passing through the switch will drop sharply. At this time, the monitoring node deployed on the switch will issue the abnormal message traffic alarm (AMTA). Besides, switches installed in smart substations generally have the function of providing an alarm when a fault occurs on the power or other boards. Therefore, if the switch itself fails, the monitoring node will also forward the STEA. It is worth noting that if we want to realize the function of message traffic statistics, it is first necessary to analyze the messages through the switch dynamically and perform message traffic statistics in the format of Table 1 [13].

Using the above fault feature information to describe the fault state has an excellent effect. For example, as shown

TABLE 1. Format of message traffic statistics.

APPID	IED Name	Type	Δt	Message traffic
0x4004	ML2211A	SV	Δt_{S1}	6M
…	…	…	…	…
0x0211	IL2211A	GOOSE	Δt_{G1}	2M
…	…	…	…	…

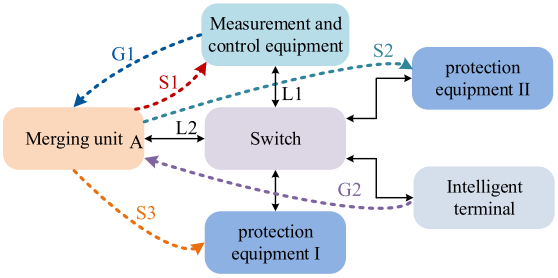

FIGURE 2. Port A of the MU is faulty.

in Figure 2, several messages are transmitted between the merging unit (MU) and other auxiliary equipment through the switch. When port A of the MU is faulty, the traffic of the message S1-S3 through the switch will drop sharply, so AMTAs of message S1-S3 will be issued. And the related auxiliary equipment will not be able to receive the message S1-S3 so that the corresponding monitoring node will issue AMRAs of message S1-S3. Also, the monitoring node located in the MU will issue AMRAs of message G1-G2 and forward the STEA. It should be noted that the above feature information is not limited to a specific fault. For example, the measurement & control equipment issues the AMRA of message S1, then the L1, L2, and equipment on the link through which the message S1 flows are all possible fault locations. Therefore, it is challenging to locate the fault point only by the traditional method. Besides, although the auxiliary equipment has the function of fault alarms, if a critical location of the communication network fails (for example, port A of the MU), some alarm signals are difficult to transmit (for example, AMRA_{G1}, AMRA_{G2}, and STEA_{MU}). Therefore, as shown in Figure 1, the redundant monitoring in the fault state proposed in this article is based on the third-party monitoring, that is, AMRAs, AMTAs, and STEAs are all counted and analyzed by the third-party system.

B. CHARACTERIZATION OF FAULT FEATURE INFORMATION UNDER REDUNDANT MONITORING

Based on the above, in the fault state of the process-level communication network, the fault section can be characterized by utilizing fault feature information from different monitoring nodes, as shown in (1):

$$X_i = [DesX_i, MidX_i], \quad i = 1, 2, \ldots N_{sum} \tag{1}$$

In (1), X_i is the set of feature information when the *i-th* fault occurs. DesX_i is the subset of the X, including the message reception state and equipment state of the message destination. MidX_i is the subset of X, including traffic statistics and

equipment state of the switch. N_{sum} is the total number of fault events.

DesX_i synthesizes the operating state of typical auxiliary equipment, as shown in (2):

$$\begin{cases} DesX_i = [MU_1, \ldots, MU_j, \ldots, MU_A, \\ P_1, \ldots, P_k, \ldots, P_B, \\ IT_1, \ldots, IT_g, \ldots, IT_C, \\ MC_1, \ldots, MC_n, \ldots, MC_D] \\ MU_j = [STEA_{MU_j}, AMRA_{j_1}, AMRA_{j_2}, \ldots, AMRA_{j_m}] \\ P_k = [STEA_{P_k}, AMRA_{k_1}, AMRA_{k_2}, \ldots, AMRA_{k_m}] \\ IT_g = [STEA_{IT_g}, AMRA_{g_1}, AMRA_{g_2}, \ldots, AMRA_{g_m}] \\ MC_n = [STEA_{MC_n}, AMRA_{n_1}, AMRA_{n_2}, \ldots, AMRA_{n_m}] \end{cases} \tag{2}$$

In (2), A, B, C, and D are the total number of MU, protection equipment, intelligent terminals, and measurement & control equipment, respectively. MU_j is the subset of DesX_i, including the message reception state and equipment state of the *j-th* MU. P_k is the subset of DesX_i, including the message reception state and equipment state of the *k-th* protection equipment. IT_g is the subset of DesX_i, including the message reception state and equipment state of the *g-th* intelligent terminal. MC_n is the subset of DesX_i, including the message reception state and equipment state of the *n-th* measurement & control equipment. During the actual operation, if MU_j cannot receive the message j_1, the monitoring node located at MU_j will issue the AMRA of message j_1, at this time, $AMRA_{j1} = 1$, otherwise $AMRA_{j1} = 0$. If MU_j itself fails, the monitoring node will forward the STEA, at this time, $STEA_{MUj} = 1$, otherwise $STEA_{MUj} = 0$.

MidX_i synthesizes the operating state of all switches in the auxiliary system and the message traffic state received by each port, as shown in (3):

$$\begin{cases} MidX_i = [S_1, \ldots, S_c, \ldots, S_N] \\ S_c = [STEA_{S_c}, Port_1, \ldots, Port_j, \ldots, Port_M] \\ Port_j = [AMTA_1, \ldots, AMTA_k, \ldots, AMTA_m] \end{cases} \tag{3}$$

In (3), N is the total number of switches. S_c is the subset of MidX_i, including traffic statistics and equipment state of the *c-th* switch, where $Port_j$ is the traffic information of *j-th* port and contains m piece of message traffic information. During the actual operation, if the traffic of message k received through $Port_j$ is too low, the switch monitoring node will issue the AMTA of message k. At this time, $AMTA_k = 1$, otherwise $AMTA_k = 0$. If S_c itself fails, the monitoring node will forward the STEA, at this time, $STEA_{Sc} = 1$, otherwise $STEA_{Sc} = 0$.

III. DESIGN OF FAULT LOCATION MODEL

Due to the fault feature information has the characteristics of large data volume and high data dimension, this article uses deep learning to establish a non-linear mapping relationship between fault features and fault locations [14], as shown in (4).

$$\begin{cases} Y = f(X) \\ X = [x_1, x_2, \ldots, x_p] \\ Y = [y_1, y_2, \ldots y_q] \end{cases} \tag{4}$$

In (4), X is the set of fault feature information, p is the dimension of the fault feature information, Y is the code of the fault location, q is the dimension of the fault location code.

A. AUTOMATIC GENERATION METHOD OF FAULT SAMPLES BASED ON EMERGENCE PRINCIPLE

According to the training rules in deep learning theory, neural networks need a large number of fault samples to get the optimal parameters. However, due to the high reliability of some equipment in the actual operating environment, the number of fault samples accumulated is tiny, so it is difficult to support the training and testing of neural networks based on the database formed by historical fault events. Therefore, in addition to the existing fault samples, other methods must be used to generate correct and reliable fault samples automatically.

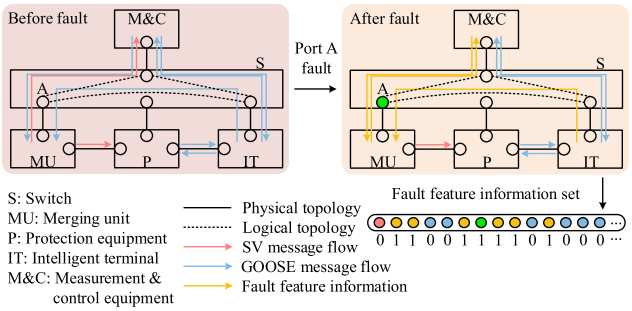

FIGURE 3. Automatic generation of fault samples.

Emergence refers to the characteristics of random behaviors that occur in the system based on the interrelationship between individuals. As shown in Figure 3, the process-level communication network at an interval is regarded as the whole system. Whether each node fails is considered as a random behavior that occurs by individuals. The topology of the communication network, the message subscription relationship, the operation of the equipment mechanism and configuration model are the interrelationship between the nodes. On this basis, if port A of the switch fails, the message reception state, the message traffic information, and the equipment operating state are the presented characteristics, which are simultaneously the fault feature information above, as shown in (5).

$$S(X) = g\left(C_{phy}, C_{\log}, C_{\bmod el}, D_{state}, E\right) \tag{5}$$

In (5), X is the set of fault feature information. C_{phy} is the physical topology of the communication network. C_{log} is the logical topology of the communication network. C_{model} is the configuration model of the communication equipment. D_{state} is the operating state of the communication equipment. E is the working environment parameter.

The fault samples generated by the above method can be stored according to (6).

$$\begin{cases} DataBase = \left[Sam_1, \ldots, Sam_j, \ldots, Sam_T\right] \\ Sam_j = \left[X_j, D_{state}, C_{phy}, C_{\log}\right] \end{cases} \tag{6}$$

In (6), T is the total number of fault samples in the database. Sam_j is the sample formed by the *j-th* fault event, which contains the set of fault feature information (X_j).

B. THE DNN-BASED MODEL FOR FAULT LOCATION

DNN improves the capabilities of feature mining and data fitting by increasing the number of hidden layers, and it is widely used in fields such as natural language processing and image analysis. Due to it increases the model depth, it is superior to shallow models in processing big data [15], [16]. Due to a large number of fault feature information and the non-linear relationship between fault features and fault types, this article uses DNN to build a fault location model for the process-level communication network.

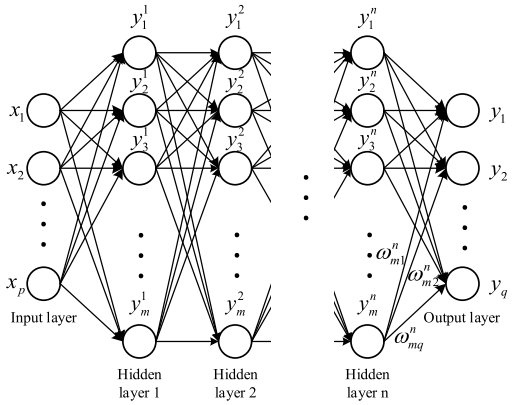

FIGURE 4. DNN topology.

As shown in Figure 4, a typical DNN includes an input layer, hidden layers, and an output layer. Among them, the input layer is the set of fault feature information, and the output layer is the code of the fault location.

During the forward propagation of DNN, neurons in the same layer are not connected. The connection mode of neurons between layers is full connection. The output of a particular neuron is shown in (7).

$$y_q^{n+1} = \sigma\left(z\right) = \sigma\left(\sum_{i=1}^{m} \omega_{iq}^n y_i^n + b_q^{n+1}\right) \tag{7}$$

In (7), y_q^{n+1} is the output of the neuron q in layer $n+1$. ω_{iq}^n is the connection weight between the neuron i in layer n and the neuron q in layer $n+1$. b_q^{n+1} is the bias of the linear relationship, where the superscript denotes the number of layers and the subscript denotes the index of the neuron. $\sigma\left(z\right)$ is the activation function, and Sigmoid can be used.

In the DNN back-propagation process, we use the loss function to measure the error between the calculated output and the actual label of the training samples. The back-propagation algorithm (BP) fine-tunes the parameters ω and b of the network by solving the minimum value of the loss function. In this article, a mini-batch learning method is used, and the loss function uses cross-entropy to improve the training speed and accuracy of the model. Therefore, the final loss function is shown in (8).

$$E\left(\theta\right) = -\frac{1}{N}\sum_{n}\sum_{q} t_{nq} \log y_{nq} \tag{8}$$

In (8), θ is the network parameter, including ω and b. N is the total number of samples. t_{nq} is the actual value of the *n-th* element in the *q-th* sample. y_{nq} is the predicted value of the *n-th* element in the *q-th* sample.

A dropout mechanism is added to the model to prevent overfitting, and it can change the structure of the neural network by randomly discarding some neurons to reduce the dependence between neurons [17]. Besides, to improve the shortcoming of the constant learning rate in the iterative process of the traditional gradient descent method, this article also uses the adaptive moment estimation (Adam) algorithm and the exponential decay method of the learning rate to update the parameters [18]. The final optimization process of the network parameter θ is shown in (9) and (10).

$$\begin{cases} g_t = \nabla_\theta E\left(\theta_{t-1}\right) \\ m_t = \beta_1 m_{t-1} + \left(1-\beta_1\right) g_t \\ v_t = \beta_2 v_{t-1} + \left(1-\beta_2\right) g_t^2 \\ \hat{m}_t = \dfrac{m_t}{1-\beta_1^t} \\ \hat{v}_t = \dfrac{v_t}{1-\beta_2^t} \\ \theta_t = \theta_{t-1} - \alpha \dfrac{\hat{m}_t}{\sqrt{\hat{v}_t} + \varepsilon} \end{cases} \tag{9}$$

$$\alpha = \alpha_0 \beta_3^{\frac{epoch-num}{N/batch-size}} \tag{10}$$

In (9) and (10), g_t is the gradient of the network parameters. m_t is the exponential moving average of the gradient. v_t is the exponential moving average of the square of the gradient. $\hat{m}_t$ and $\hat{v}_t$ are the corrected quantities. β_1, β_2, and β_3 are the exponential decay rates, which are taken as 0.9, 0.999, and 0.95, respectively. α_0 is the initial value of the learning rate. *epoch-num* is the current training times. *batch-size* is the batch processing parameter.

IV. STEPS OF FAULT LOCATION

Based on the above, a fault location framework of process-level communication networks is shown in Figure 5. The specific steps are:

1) A determination process for triggering the fault location model is set to eliminate the interference of a small number of error alarms. When the total number of fault feature information is detected to be higher than a threshold value, the fault location model is triggered. The threshold value of this process is set to the minimum amount of alarm information at the time of the historical fault.

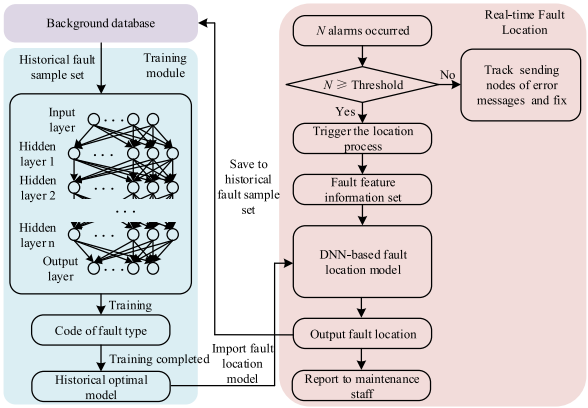

FIGURE 5. Fault location framework.

2) The fault feature information of each monitoring node is called to form X when the process-level communication network is faulty.
3) The X is used as the input of the neural network and sent to the DNN model to obtain the fault localization result.

V. SIMULATION EXAMPLE

A. INTRODUCTION TO SIMULATION

A typical process-level communication network of 110kV smart substation is simulated to verify the effectiveness of the fault location method proposed in this article, and its topology is shown in Figure 6. The auxiliary system consists of two line-intervals, two transformer-intervals, and one bus-interval. Each interval contains the auxiliary equipment and the fiber-optic links. To simulate the complex linking that may occur in the actual working environment, the communication network in the example uses a ''point to point'' way within the interval, and the remaining GOOSE/SV messages are separately networked [19]. The equipment name, port number, and link number has been given. The GOOSE/SV messages transmitted in the network are shown in Table 2.

B. CONSTRUCTION AND OPTIMIZATION OF DNN MODEL

In this simulation scenario, according to the representation method of fault feature information and the information in Tables 2 and Table 3, it is known that the destination-based alarms have 112 elements, including 86 AMRAs and 26 STEAs. The switch-based alarms have 151 elements, including 146 AMTAs and 5 STEAs. Therefore, the total number of neurons in the input layer is set to 263. According to the description of the fault location of the communication network, it is known that the 92 equipment ports and 46 fiber-optic links are all possible fault locations, so the total number of output layer neurons is set to 138. It is particularly pointed out that if all ports of specific equipment are judged to be faulty, there is reason to highly suspect that the I/O module of this equipment or even the entire equipment is defective.

Based on the aforementioned automatic generation method of fault samples, the samples obtained for each fault type are divided into training samples (about 80%) and test samples (about 20%). The neural network is optimized by setting different hyper-parameters, and the optimal hyper-parameters are selected with the discrimination accuracy of the training samples. The results are as follows.

TABLE 2. GOOSE/SV messages transmitted in the network.

Message type	Message number	Publish port	Subscription Port
GOOSE	G1-G6	1	7,13,14,27,52,77
	G7-G9	13	1,7,88
	G10-G15	14	1,20,26,27,52,77
	G16-G18	26	14,20,88
	G19-G27	27	1,14,36,39,40,42,51,52,77
	G28	40	27
	G29-G31	42	27,36,88
	G32-G34	51	27,39,88
	G35-G43	52	1,14,27,61,63,66,67,76,77
	G44	63	52
	G45-G47	67	52,61,88
	G48-G50	76	52,66,88
	G51-G55	77	1,14,27,52,91
	G56-G65	88	9,13,22,26,42,44,51,67,69,76
	G66-G67	91	86,77
SV	S1-S2	7	1,88
	S3-S4	20	14,88
	S5-S6	36	27,88
	S7-S8	39	27,88
	S9-S10	61	52,88
	S11-S12	66	52,88
	S13-19	86	7,20,36,39,61,66,77

It can be seen from Figure 7 that under the premise of fixed initial learning rates and batch-size, the optimization effect of the neural network is best when there are one hidden layer and 512 neurons. Increasing the number of hidden layers and the number of neurons contained in each layer will increase the difficulty of training the neural network, although the initial convergence rate is relatively fast, the final training accuracy is lower. When the number of hidden layers and the number of neurons is small, the fitting performance of the neural network is weak, and the convergence speed is slow.

It can be seen from Figure 8 that after determining the number of hidden layers and the number of neurons, $\alpha_0 = 0.07$ and batch-size=256 are the best for the neural network. When the α_0 is larger, the convergence speed is slightly faster. Still, the final training accuracy rate is worse. When the α_0 is smaller, the convergence speed of the neural network is significantly reduced, and the ultimate training accuracy rate is reduced. Increasing batch-size can improve the accuracy of the training. Still, when it rises to a certain degree, its impact on the accuracy is minimal, and the training time of the neural network is greatly extended. Besides, with the increase of the number of iterations within a specific range, the training accuracy rate of the neural network will continue to improve. Still, when the number of iterations rises to a certain degree, the

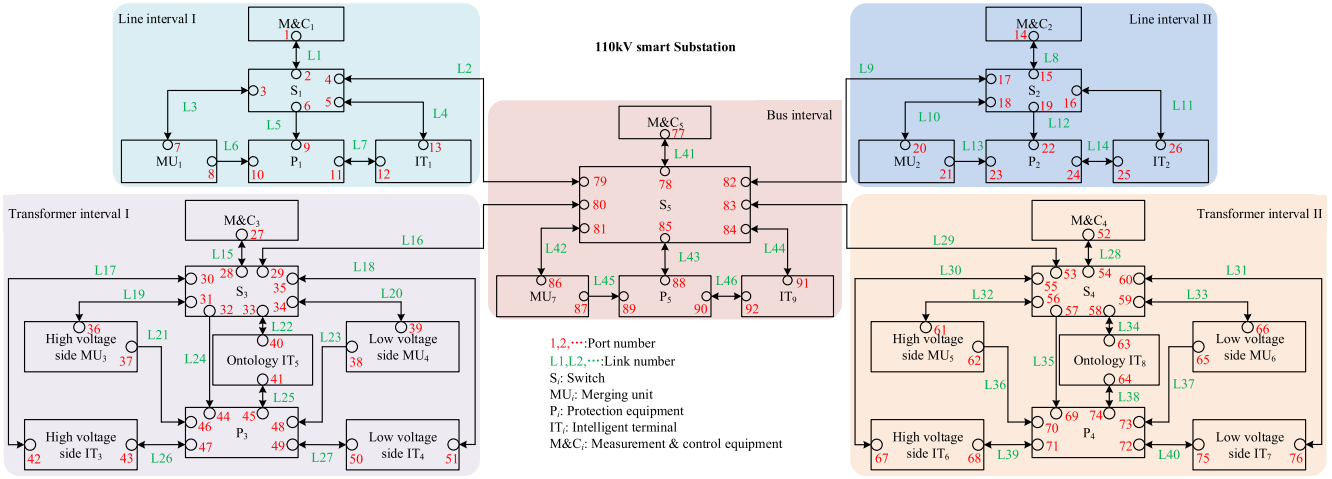

FIGURE 6. The process-level communication network of 110kV smart substation.

TABLE 3. Messages received through each port of the switch.

Switch number	Port number	Message number
S_1	2	G1/G2/G3/G4/G5/G6
	3	S1/S2
	4	G10/G19/G35/G51/G56/G57/S13
	5	G7/G8/G9
S_2	15	G10/G11/G12/G13/G14/G15
	16	G16/G17/G18
	17	G3/G20/G36/G52/G58/G59/S14
	18	S3/S4
S_3	28	G19/G20/G21/G22/G23/G24/G25/G26/G27
	29	G4/G13/G37/G53/G60/G61/G62/S15/S16
	30	G29/G30/G31
	31	S5/S6
	33	G28
	34	S7/S8
	35	G32/G33/G34
S_4	53	G5/G14/G26/G54/G63/G64/G65/S17/S18
	54	G35/G36/G37/G38/G39/G40/G41/G42/G43
	55	G45/G46/G47
	56	S9/S10
	58	G44
	59	S11/S12
	60	G48/G49/G50
S_5	78	G51/G52/G53/G54/G55
	79	G3/G4/G5/G6/G9/S2
	80	G19/G20/G26/G27/G31/G34/S6/S8
	81	S13/S14/S15/S16/S17/S18/S19
	82	G10/G13/G14/G15/G18/S4
	83	G35/G36/G37/G43/G47/G50/S10/S12
	84	G66/G67
	85	G56/G57/G58/G59/G60/G61/G62/G63/G64/G65

training accuracy rate will become stable. So, the maximum value after the training accuracy rate stabilizes is selected to reduce the training time and resource loss of the model, which

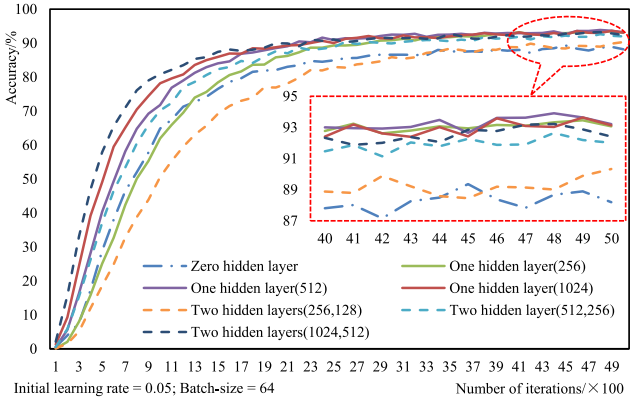

FIGURE 7. Effects of hidden layers and neurons on neural network optimization.

is the best when the number of iterations is 4600. At this time, the training accuracy rate is 96.467%.

In summary, the main hyper-parameters of DNN are shown in Table 4:

VI. EXPERIMENTAL RESULTS

The following analysis is carried out from a single fault, multiple faults, and unreliable fault feature information to show the effectiveness of the DNN model in various environments, and the DNN model is compared with the traditional fault location method.

A. RESULTS IN SINGLE FAULT ENVIRONMENTS

The single fault environment means that there is only one fault point at the same time. The verification of the test set can analyze the effectiveness of the DNN model in single fault environments, as shown in Figure 9.

It can be seen from Figure 9 that the DNN model has an excellent recognition effect for each fault type in the test set, and the accuracy rate is maintained at 97.5% $\sim$ 100%. The average location accuracy rate of the fiber-optic fault is 98.972%, and the average location accuracy rate of the port

TABLE 4. The main hyper-parameters of DNN.

Hyper-parameters	Value
Number of input layer nodes	263
Number of hidden layers	1
Number of hidden layer nodes	512
Number of output layer nodes	138
Activation function	Sigmoid
Loss function	Cross-entropy
Initial learning rate	0.07
Batch-size	256
Dropout	0.1
Number of iterations	4600

TABLE 5. Message traffic affected by the fault of fiber-optic L2.

Switch number	Port number	Message number
1	4	G10/G19/G35/G51/G56/G57/S13
2	17	G3
3	29	G4
4	53	G5
5	79	G3/G4/G5/G6/G9/S2

fault is 99.139%. The overall accuracy rate of all test samples reaches 99.072%, which meets the actual engineering need.

For real-time fault location, it takes the fiber-optic L2 fault in Figure 6 as an example. After the fault occurs, as shown in Table 5, the traffic of these messages will drop sharply, which will trigger the AMTAs of these messages. Besides, the related auxiliary equipment will also issue AMRAs because they cannot regularly receive these messages. Therefore, DesX and MidX in the set X composed of the above alarms are as shown in (11) and (12). (Due to a large amount of data, only non-zero term position elements are listed.)

$$\begin{cases} DesX = [MU_1, P_1, P_5, IT_1, \\ MC_1, MC_2, MC_3, MC_4, MC_5] \\ MU_1 = [AMRA_{S13}], IT_1 = [AMRA_{G57}] \\ P_1 = [AMRA_{G56}], P_5 = [AMRA_{G9}, AMRA_{S2}] \\ MC_1 = [AMRA_{G10}, AMRA_{G19}, AMRA_{G35}, AMRA_{G51}] \\ MC_2 = [AMRA_{G3}], MC_3 = [AMRA_{G4}] \\ MC_4 = [AMRA_{G5}], MC_5 = [AMRA_{G6}] \end{cases} \tag{11}$$

$$\begin{cases} MidX = [S_1, S_2, S_3, S_4, S_5] \\ S_1 = [Port_4] \\ Port_4 = [AMTA_{G10}, AMTA_{G19}, AMTA_{G35}, \\ AMTA_{G51}, AMTA_{G56}, AMTA_{G57}, AMTA_{S13}] \\ S_2 = [Port_{17}], Port_{17} = [AMTA_{G3}] \\ S_3 = [Port_{29}], Port_{29} = [AMTA_{G4}] \\ S_4 = [Port_{53}], Port_{53} = [AMTA_{G5}] \\ S_5 = [Port_{79}] \\ Port_{79} = [AMTA_{G3}, AMTA_{G4}, AMTA_{G5}, \\ AMTA_{G6}, AMTA_{G9}, AMTA_{S2}] \end{cases} \tag{12}$$

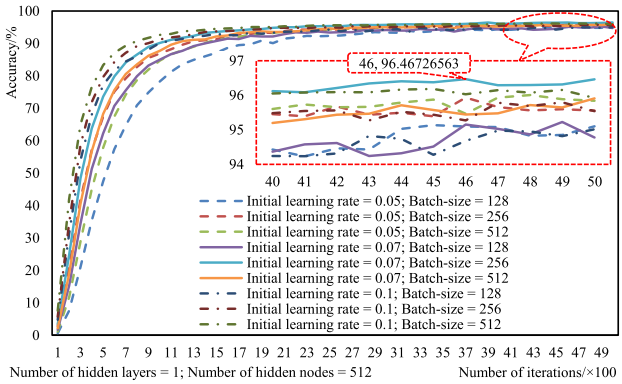

FIGURE 8. Effects of bath-size and initial learning rate on neural network optimization.

The location result Y obtained is shown in (13) by using the set X as input to the optimal DNN model (The output layer threshold is set to 0.9):

$$Y_{DNN} = \begin{bmatrix} L2 \\ 0, \ldots, 1, \ldots, 0 \end{bmatrix} \tag{13}$$

Traditional fault location approaches take the cross-path method and the flow-criterion method as examples [8-9].

The cross-path method only locates faults based on the state of message reception. In this example, by some auxiliary equipment that cannot regularly receive the messages (G3, G4, G5, G6, G9, G10, G19, G35, G51, G56, G57, S2, and S13), the fault location result obtained is shown in (14):

$$Y_{cross-path} = \begin{bmatrix} L2Port4Port79 \\ 0, \ldots, 1, \ldots, 1, \ldots, 1, \ldots, 0 \end{bmatrix} \tag{14}$$

The flow-criterion method only locates faults based on the state of message traffic. In this example, the traffic of some messages (G3, G4, G5, G6, G9, G10, G19, G35, G51, G56, G57, S2, and S13) through the switch drops sharply, so the fault location result obtained is shown in (15):

$$Y_{flow-criterion} = \begin{bmatrix} L2Port2Port4Port79 \\ 0, \ldots, 1, \ldots, 1, \ldots, 1, \ldots, 1, \ldots, 0 \end{bmatrix} \tag{15}$$

The relative error between the actual fault range and the suspected fault range is used as an evaluation index to compare the effects of different methods, as shown in (16):

$$Er\left(\hat{Y}\right) = \frac{\left|Y - \left(Y \cap \hat{Y}\right)\right|}{|Y|} \tag{16}$$

In (15), Y is the suspected fault range. $\hat{Y}$ is the actual fault range. Specify $|Y|$ as the number of non-zero elements in the set Y.

According to the calculation method of relative error, when the L2 fails, the relative error of the DNN model proposed in this article is 0. Still, the relative errors of the cross-path method and flow-criterion method are 0.667 and 0.75 respectively. It can be seen that the method proposed in this article can effectively reduce the suspected fault range by using

TABLE 6. Comparison of three methods in single fault environments.

Method	Accuracy	Maximum error	Minimum error	Average error
DNN	99.072%	0.5	0	0.004
Cross-path	80.692%	0.889	0	0.249
Flow-criterion	77.644%	0.875	0	0.314

multidimensional features and DNN to improve the efficiency of operation and maintenance.

According to the above fault location process and the calculation method of relative error, fault analysis and error calculation are carried out for all fault events in the test sample set by the DNN model, the cross-path method, and flow-criterion method. The maximum error, the minimum error, and the average error of the two methods are compared, as shown in Table 6.

It can be known from Table 6 that the average error and the maximum error of the DNN model are both lower than the cross-path method and flow-criterion method, so the DNN model can significantly improve the accuracy of fault location. The reason for this result is enlarging the dimension of the fault feature information and adopting a more reasonable method to process multidimensional data.

B. RESULTS IN MULTIPLE FAULT ENVIRONMENTS

The multiple fault environment refers to the existence of two or more fault points at the same time. These fault points may be located at the same interval or at different intervals.

Take the port 7 of MU 1 and the port 88 of protection equipment 5 in Figure 6 as an example. When two ports fail at the same time, as shown in Table 7, the traffic of these messages will be significantly reduced, thus triggering AMTAs. Besides, some auxiliary equipment that subscribes the messages (G1, G8, G9, G18, G31, G34, G47, G50, G56, G57, G58, G59, G60, G61, G62, G63, G64, G65, S1, S2, S4, S6, S8, S10, S12, and S13) will send AMRAs. The MU 1 and the protection equipment 5 will also issue STEAs. Therefore, DesX and MidX in the set X composed of the above alarms are as shown in (17) and (18). (Due to a large amount of data, only non-zero term position elements are listed.)

$$\begin{cases} DesX = [MU_1, P_1, P_2, P_3, P_4, P_5, \\ IT_1, IT_2, IT_3, IT_4, IT_6, IT_7] \\ MU_1 \\ = \left[STEA_{MU_1}, AMRA_{G1}, AMRA_{G8}, AMRA_{S1}, AMRA_{S13}\right] \\ P_1 = [AMRA_{G56}], P_2 = [AMRA_{G58}] \\ P_3 = [AMRA_{G61}], P_4 = [AMRA_{G64}] \\ P_5 = \left[STEA_{P_5}, AMRA_{G9}, AMRA_{G18}, AMRA_{G31}, \right. \\ AMRA_{G34}, AMRA_{G47}, AMRA_{G50}, AMRA_{S2}, AMRA_{S4}, \\ \left. AMRA_{S6}, AMRA_{S8}, AMRA_{S10}, AMRA_{S12}\right] \\ IT_1 = [AMRA_{G57}], IT_2 = [AMRA_{G59}], IT_3 = [AMRA_{G60}] \\ IT_4 = [AMRA_{G62}], IT_6 = [AMRA_{G63}], IT_7 = [AMRA_{G65}] \end{cases} \tag{17}$$

TABLE 7. Message traffic affected by faults of port 7 and port 88.

Switch number	Port number	Message number
1	3	S1-S2
	4	G56-G57
2	17	G58-G59
3	29	G60-G62
4	53	G63-G65
5	79	G3/G4/G5/G6/G9/S2
	85	G56-G65

$$\begin{cases} MidX = [S_1, S_2, S_3, S_4, S_5] \\ S_1 = [Port_3, Port_4] \\ Port_3 = [AMTA_{S1}, AMTA_{S2}] \\ Port_4 = [AMTA_{G56}, AMTA_{G57}] \\ S_2 = [Port_{17}], Port_{17} = [AMTA_{G58}, AMTA_{G59}] \\ S_3 = [Port_{29}], Port_{29} = [AMTA_{G60}, AMTA_{G61}, AMTA_{G62}] \\ S_4 = [Port_{53}], Port_{53} = [AMTA_{G63}, AMTA_{G64}, AMTA_{G65}] \\ S_5 = [Port_{79}, Port_{85}], Port_{79} = [AMTA_{S2}] \\ Port_{85} = [AMTA_{G56}, AMTA_{G57}, AMTA_{G58}, \\ AMTA_{G59}, AMTA_{G60}, AMTA_{G61}, \\ AMTA_{G62}, AMTA_{G63}, AMTA_{G64}, AMTA_{G65}] \end{cases} \tag{18}$$

The location result Y obtained is shown in (19) by using the set X as input to the optimal DNN model (The output layer threshold is set to 0.9):

$$Y_{DNN} = \begin{bmatrix} Port7Port88 \\ 0, \ldots, 1, \ldots, 1, \ldots, 0 \end{bmatrix} \tag{19}$$

According to the analysis process of the cross-path method, it locates faults based on the reception state of the messages sent by port 7 and port 88, respectively. However, since the transmission path of the message S1 sent from port 7 and the transmission path of all the messages sent from port 88 have no intersection, so the location result is an empty set, and the relative error is 1. According to the analysis process of the flow-criterion method, the traffic of some messages (G56-G65, S1, and S2) through the switch drops sharply, so the fault location result obtained is shown in (20), and the relative error is 0.667, while the relative error of the DNN model is 0.

$$Y_{flow-criterion} = \begin{bmatrix} L3L43Port3Port85 \\ 0, \ldots, 1, \ldots, 1, \ldots, 1, \ldots, 1, \ldots, 1, \ldots, 1, \ldots, 0 \\ Port7Port88 \end{bmatrix} \tag{20}$$

One hundred sets of samples were randomly simulated to verify the general location effect of the DNN model in multiple fault environments. According to the above fault location process and the calculation method of relative error, fault analysis and error calculation are carried out for all fault samples by the DNN model, the cross-path method, and the flow-criterion method. The results are shown in Table 8.

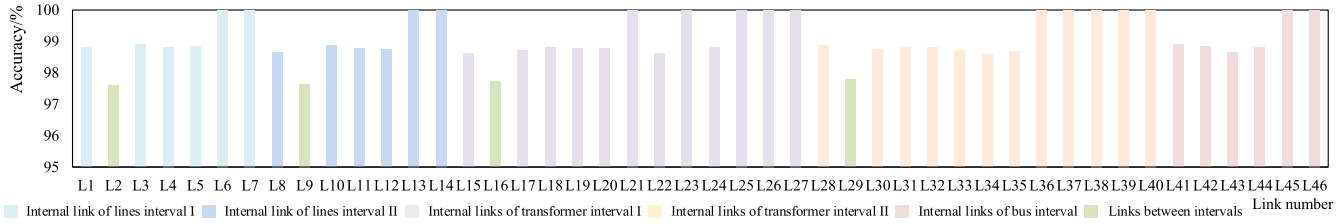

(a) The fault of fiber-optic links

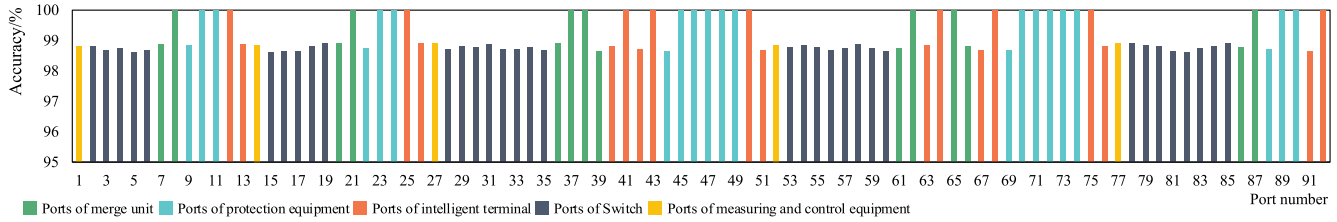

(b) The fault of ports

FIGURE 9. Results in single fault environments.

TABLE 8. Comparison of three methods in multiple fault environments. (a) Two fault points. (b) Three fault points

(a) Two fault points

Method	Accuracy	Maximum error	Minimum error	Average error
DNN	92%	0.333	0	0.027
Cross-path	41%	1	0	0.558
Flow-criterion	0%	1	0.333	0.607

(b) Three fault points

Method	Accuracy	Maximum error	Minimum error	Average error
DNN	86%	0.25	0	0.035
Cross-path	36%	1	0	0.632
Flow-criterion	0%	1	0.25	0.694

It can be known from Table 8 that the relative error of the DNN model is lower than other methods, while the accuracy of the DNN model is higher than other methods. With the increase of the fault complexity, although the average error of the DNN model increases slightly, considering that the probability of multiple faults in the actual operating environment is low, hence, the DNN model still has a reliable fault location capability.

C. ANALYSIS OF ANTI-INTERFERENCE ABILITY WITH UNRELIABLE FAULT FEATURE INFORMATION

Unreliable fault feature information refers to the situation in which fault feature information is incorrect or lost. The anti-interference ability of the DNN model is discussed below.

Taking the fault of the fiber-optic L2 as an example. After the fault occurs, if the intelligent terminal 1 incorrectly reports the AMRA of message G2, and the remaining fault feature information is correct, then, DesX and MidX in the set X are shown in (21) and (22). (Due to a large amount of data, only non-zero position elements are listed.)

$$\begin{cases} DesX = [MU_1, P_1, P_5, IT_1, \\ MC_1, MC_2, MC_3, MC_4, MC_5] \\ MU_1 = [AMRA_{S13}], IT_1 = [AMRA_{G2}, AMRA_{G57}] \\ P_1 = [AMRA_{G56}], P_5 = [AMRA_{G9}, AMRA_{S2}] \\ MC_1 = [AMRA_{G10}, AMRA_{G19}, AMRA_{G35}, AMRA_{G51}] \\ MC_2 = [AMRA_{G3}], MC_3 = [AMRA_{G4}] \\ MC_4 = [AMRA_{G5}], MC_5 = [AMRA_{G6}] \end{cases} \tag{21}$$

$$\begin{cases} MidX = [S_1, S_2, S_3, S_4, S_5] \\ S_1 = [Port_4] \\ Port_4 = [AMTA_{G10}, AMTA_{G19}, AMTA_{G35}, \\ AMTA_{G51}, AMTA_{G56}, AMTA_{G57}, AMTA_{S13}] \\ S_2 = [Port_{17}], Port_{17} = [AMTA_{G3}] \\ S_3 = [Port_{29}], Port_{29} = [AMTA_{G4}] \\ S_4 = [Port_{53}], Port_{53} = [AMTA_{G5}] \\ S_5 = [Port_{79}] \\ Port_{79} = [AMTA_{G3}, AMTA_{G4}, AMTA_{G5}, \\ AMTA_{G6}, AMTA_{G9}, AMTA_{S2}] \end{cases} \tag{22}$$

The location result Y obtained is shown in (23) by using the set X as input to the optimal DNN model (The output layer threshold is set to 0.9):

$$Y_{DNN} = \begin{bmatrix} L2 \\ 0, \ldots, 1, \ldots, 0 \end{bmatrix} \tag{23}$$

According to the analysis process of the cross-path method, the fault location result is shown in (24). The fault location result of the flow-criterion method is still shown in (15).

$$Y_{cross-path} = \begin{bmatrix} L2L4Port4Port13 \\ 0, \ldots, 1, \ldots, 1, \ldots, 1, 1, \ldots, 1, \ldots, 1, \ldots, 0 \\ Port5Port79 \end{bmatrix} \tag{24}$$

TABLE 9. Comparison of three methods in unreliable fault feature information environments.

Method	Accuracy	Maximum error	Minimum error	Average error
DNN	96%	0.333	0	0.013
Cross-path	52%	1	0	0.438
Flow-criterion	44%	1	0	0.517

At this time, the relative error of the cross-path method is 0.833, and the relative error of the flow-criterion method is 0.75, while the relative error of the DNN model is still 0. The reason is that the false AMRA of message G2 and the AMRA of message G57 cause the fiber-optic L4 and the ports on both sides to be mistakenly regarded as fault points in the cross-path method. However, the DNN model takes into account the message traffic conditions of the switch, since the monitoring node located in the port 2 of switch 1 does not issue the AMTA of message G2, the weight of false AMRA of message G2 is weakened. It can be seen that the cross-path method is hugely susceptible to the confidence of the feature information. Still, the use of redundant detection can help improve the anti-interference ability of the fault location model.

One hundred sets of fault samples are selected in the test set to discuss whether the DNN model has general anti-interference ability, these fault samples can obtain correct location results through the DNN model, the cross-path method and the flow-criterion method. Randomly set a piece of feature information belonging to DesX or MidX in each group of samples to "0" (initially "1") or "1" (initially "0") to simulate an environment where the feature information is unreliable. Taking the DNN model, the flow-criterion method, and the cross-path method to analyze the processed samples, and the results are shown in Table 9.

As can be seen from Table 9, the relative error of the DNN model is lower than other methods, while the accuracy of the DNN model is higher than other methods, so it has an excellent anti-interference ability in the environments where the feature information is wrong or missing. Besides, it should be noticed whether different information confidence will affect fault location results. In the future, it will also be possible to consider adding information certification to eliminate incorrect fault location results caused by tampering or damaging information during external malicious invasion [20].

VII. CONCLUSION

With the process-level communication network of smart substations is becoming more sophisticated, aiming at the problem that the fault is challenging to be accurately located, this article proposes a method for fault location of process-level communication networks based on DNN. First of all, based on the redundant monitoring of the fault state, the feature information obtained by the monitoring nodes in different positions is analyzed, and the characterization method of fault feature information is proposed. Secondly, based on the emergence principle, a large number of fault samples are automatically generated to expand the training set. Finally, combined with the training rules in deep learning theory, a fault location model of process-level communication networks based on DNN is established, and the real-time location steps are given.

Simulation results show that the DNN model can handle high-dimensional sets of fault feature information and accurately locate faults in various fault environments. Besides, under the influence of loss or error of feature information, the DNN model can still accurately determine the fault point and has an excellent anti-interference ability. So, the DNN model can reduce the impact of the information confidence on the fault location in the increasingly complex operating environment. The next work can be carried out from three aspects, one is to select a better deep learning algorithm to optimize the model [21]–[23]; the second is to consider more diverse communication network structures, such as ring topology; the third is to expand the scope of fault identification to achieve the overall state monitoring of the smart substation auxiliary system.

ACKNOWLEDGMENT

(Bo Ren and Jinsong Li contributed equally to this work.)

REFERENCES

[1] H. Wang, B. Zhou, and X. Zhang, "Research on the remote maintenance system architecture for the rapid development of smart substation in China," *IEEE Trans. Power Del.*, vol. 33, no. 4, pp. 1845–1852, Aug. 2018.
[2] X. Dong, D. Wang, M. Zhao, B. Wang, S. Shi, and A. Apostolov, "Smart power substation development in China," *CSEE J. Power Energy Syst.*, vol. 2, no. 4, pp. 1–5, Dec. 2016.
[3] T. Skeie, S. Johannessen, and C. Brunner, "Ethernet in substation automation," *IEEE Control Syst.*, vol. 22, no. 3, pp. 43–51, Jun. 2002.
[4] Y. Zhang, Z. Cai, X. Li, and R. He, "Analytical modeling of traffic flow in the substation communication network," *IEEE Trans. Power Del.*, vol. 30, no. 5, pp. 2119–2127, Oct. 2015.
[5] C. R. Ozansoy, A. Zayegh, and A. Kalam, "The real-time publisher/subscriber communication model for distributed substation systems," *IEEE Trans. Power Del.*, vol. 22, no. 3, pp. 1411–1423, Jul. 2007.
[6] Y. Xi, J. Zhou, Z. Cai, and Z. Su, "Information security protection method for smart substation communication network based on message identification and flow control," (in Chinese), *Power Syst. Technol.*, vol. 41, no. 2, pp. 624–629, Feb. 2017.
[7] B. Li, J. Yang, B. Qi, Y. Sun, H. Yan, and S. Chen, "Application of *p*-cycle protection for the substation communication network under SRLG constraints," *IEEE Trans. Power Del.*, vol. 29, no. 6, pp. 2510–2518, Dec. 2014.
[8] L. Luo, Q. Peng, D. Wang, C. Li, and J. Shen, "Monitoring method of process level network in smart substation," (in Chinese), *Autom. Electr. Power Syst.*, vol. 42, no. 11, pp. 151–156, Jun. 2018.
[9] Y. Zhang, Z. Cai, P. Long, X. Li, and Z. Su, "Real-time fault diagnosis models and method for communication network in smart substation," (in Chinese), *Power Syst. Technol.*, vol. 40, no. 6, pp. 1851–1857, Jun. 2016.
[10] C. T. Law, K. Bhattarai, and D. C. Yu, "Fiber-optics-based fault detection in power systems," *IEEE Trans. Power Del.*, vol. 23, no. 3, pp. 1271–1279, Jul. 2008.
[11] F. Salvadori, C. S. Gehrke, A. C. de Oliveira, M. de Campos, and P. S. Sausen, "Smart grid infrastructure using a hybrid network architecture," *IEEE Trans. Smart Grid*, vol. 4, no. 3, pp. 1630–1639, Sep. 2013.
[12] Q. Yang, W. Hao, L. Ge, W. Ruan, and F. Chi, "FARIMA model-based communication traffic anomaly detection in intelligent electric power substations," *IET Cyber-Phys. Syst., Theory Appl.*, vol. 4, no. 1, pp. 22–29, Mar. 2019.
[13] T. Yang, R. Zhao, W. Zhang, and Q. Yang, "On the modeling and analysis of communication traffic in intelligent electric power substations," *IEEE Trans. Power Del.*, vol. 32, no. 3, pp. 1329–1338, Jun. 2017.

[14] S. S. Gururajapathy, H. Mokhlis, and H. A. Illias, "Fault location and detection techniques in power distribution systems with distributed generation: A review," *Renew. Sustain. Energy Rev.*, vol. 74, pp. 949–958, Jul. 2017.
[15] S. Naseer, Y. Saleem, S. Khalid, M. K. Bashir, J. Han, M. M. Iqbal, and K. Han, "Enhanced network anomaly detection based on deep neural networks," *IEEE Access*, vol. 6, pp. 48231–48246, 2018.
[16] M. Mirzaei, B. Vahidi, and S. H. Hosseinian, "Fault location on a series-compensated three-terminal transmission line using deep neural networks," *IET Sci., Meas. Technol.*, vol. 12, no. 6, pp. 746–754, Sep. 2018.
[17] B. Ko, H.-G. Kim, K.-J. Oh, and H.-J. Choi, "Controlled dropout: A different approach to using dropout on deep neural network," in *Proc. IEEE Int. Conf. Big Data Smart Comput. (BigComp)*, Jeju-do, South Korea, Feb. 2017, pp. 358–362.
[18] Z. Zhang, "Improved adam optimizer for deep neural networks," in *Proc. IEEE/ACM 26th Int. Symp. Qual. Service (IWQoS)*, Banff, AB, Canada, Jun. 2018, pp. 1–2.
[19] H. Hajian-Hoseinabadi, "Availability comparison of various power substation automation architectures," *IEEE Trans. Power Del.*, vol. 28, no. 2, pp. 566–574, Apr. 2013.
[20] A. Chattopadhyay, A. Ukil, D. Jap, and S. Bhasin, "Toward threat of implementation attacks on substation security: Case study on fault detection and isolation," *IEEE Trans. Ind. Informat.*, vol. 14, no. 6, pp. 2442–2451, Jun. 2018.
[21] K. He, X. Zhang, S. Ren, and J. Sun, "Deep residual learning for image recognition," in *Proc. IEEE Conf. Comput. Vis. Pattern Recognit. (CVPR)*, Las Vegas, NV, USA, Jun. 2016, pp. 770–778.
[22] K. Jiang, Z. Wang, P. Yi, G. Wang, K. Gu, and J. Jiang, "ATMFN: Adaptive-threshold-based multi-model fusion network for compressed face hallucination," *IEEE Trans. Multimedia*, early access, Dec. 18, 2020, doi: 10.1109/TMM.2019.2960586.
[23] K. Jiang, Z. Wang, P. Yi, G. Wang, T. Lu, and J. Jiang, "Edge-enhanced GAN for remote sensing image superresolution," *IEEE Trans. Geosci. Remote Sens.*, vol. 57, no. 8, pp. 5799–5812, Aug. 2019.

BO REN was born in Nanchong, Sichuan, China, in 1996. He received the B.Eng. degree in electrical engineering and automation from North China Electric Power University, Baoding, China, in 2018, where he is currently pursuing the M.Eng. degree in electrical engineering.

His research interests include data processing and state detection of smart substations.

JINSONG LI was born in Hefei, Anhui, China, in 1981. He received the M.Eng. degree from North China Electric Power University, Beijing, China, in 2016.

He is currently a Senior Engineer with the China Electric Power Research Institute, Beijing. His research interests include power system automation and smart grid security.

YONGKANG ZHENG received the Ph.D. degree in electrical engineering from Southwest Jiaotong University, Chengdu, China, in 2018.

He is currently a Professor-Level Senior Engineer with the State Grid Sichuan Electric Power Research Institute, Chengdu. His research interests include the smart grid and smart substation.

XIAODONG CHEN was born in Luzhou, Sichuan, China, in 1976. He received the M.Eng. degree in electrical engineering from Sichuan University, Chengdu, China, in 2011.

He is currently a Senior Engineer with State Grid Sichuan Electric Power Company, Chengdu. His research interests include relay protection, grid planning, and infrastructure management.

YIBING ZHAO received the M.Eng. degree in software engineering from the University of Electronic Science and Technology of China, Chengdu, China, in 2011.

He is currently a Senior Engineer with State Grid Sichuan Electric Power Company, Chengdu. His research interest includes electricity information.

HAIYANG ZHANG was born in Fuyang, Anhui, China, in 1994. He received the B.Eng. degree in electrical engineering and automation from Sichuan University, Chengdu, China, in 2018, where he is currently pursuing the M.Eng. degree in electrical engineering.

His research interest includes the visualization and automation of the auxiliary system of smart substations.

CHAO ZHENG was born in Meishan, Sichuan, China, in 1995. He received the B.Eng. degree in electrical engineering and automation from Chengdu University, Chengdu, China, in 2018. He is currently pursuing the M.Eng. degree in electrical engineering with Sichuan University, Chengdu.

His research interest includes the protection and control of the power systems.